ACS OMEGA

http://pubs.acs.org/journal/acsodf

Article

Synthesis of Ni−B Compounds by High-Pressure and High-Temperature Method

Guiqian Sun, Xingbin Zhao, Lu Chen, Yubo Fu, Wei Zhao, Meiyan Ye, Fei Wang, Qiang Tao,* Shushan Dong,* and Pinwen Zhu*

Cite This: *ACS Omega* 2023, 8, 9265−9274

Read Online

ACCESS | Metrics & More | Article Recommendations | Supporting Information

ABSTRACT: Nickel borides are promising multifunctional materials for high hardness and excellent properties in catalysis and magnetism. However, it is still a blank of intrinsic properties in Ni−B compounds, because crystallization of the single phases of Ni−B compounds with micro-size is a challenge. In this work, single phases of Ni_2B (*I*4/*mcm*), α-Ni_4B_3 (*Pnma*), β-Ni_4B_3 (*C*2/*c*), and NiB (*Cmcm*) are synthesized by high pressure and high temperature (HPHT). The results indicate that synthesizing α-Ni_4B_3 and β-Ni_4B_3 requires more energy than Ni_2B and NiB. The growth process of Ni−B compounds is that Ni covers B to form Ni−B compounds under HPHT, which also makes the slight excess of B necessary. So, generating homogeneous distribution of starting materials and increasing the interdiffusion between Ni and B are two keys to synthesize well crystallized and purer samples by HPHT. This work uncovers the growth process of Ni−B compounds, which is significant to guide the synthesis of highly crystalline transition metal borides (TMBs) in the future.

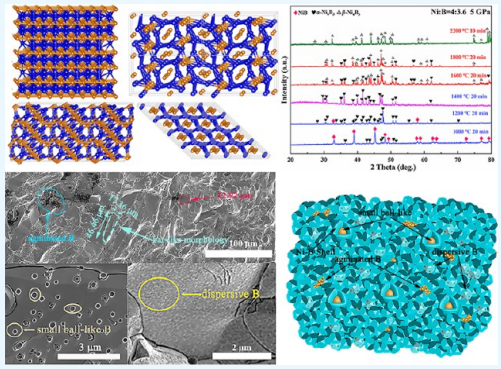

1. INTRODUCTION

Nickel borides are promising functional materials, because of their potential high hardness, high melting point, high thermal stability, and excellent catalytic performance.[1−5] The superior properties are from Ni and B atoms that can construct abundant subunits, which contribute to form rich Ni−B compounds.[6−8] However, there are rarely reports of single phases of Ni−B compounds which have good crystallization, especially the bulk samples of Ni−B compounds. There is still a lack of data on the intrinsic properties of Ni−B compounds, such as conductivity and hardness. It is also an obstacle to understanding the mechanism of functional properties of Ni−B compounds.[9] Hence, it is urgent to synthesize single phases of Ni−B compounds to further uncover a new kind of functional material.

The intrinsic reason for lacking Ni−B compounds is that synthesis of Ni−B compounds needs to overcome a high energy barrier due to the chemical inertness of nickel and boron.[8,10−12] The grain growth of Ni−B compounds is slow in which they always form amorphous or nanosized compounds by conventional experimental methods. For example, Liaw et al. only synthesized amorphous NiB by using nickel acetate with sodium boride under atmosphere pressure. Nanoscale Ni−B compounds can be synthesized by $NiCl_2$ and $NaBH_4$ which heat at 750 °C for 1.5 h.[13] However, there are many defects and stacking faults appearing in the nanoparticles. Another problem is that the mixed phases are easily generated in the synthesis of Ni−B compounds, such as Ni,[7] Ni_3B,[10] and Ni_4B_3.[8] The reason for mixtures is that the substructures of Ni−B compounds are very close and all of the Gibbs free energies of NiB compounds are negative at temperature of 0−1200 K, which means all the Ni−B compounds can be spontaneously reacted by elements Ni and B. Meanwhile, the products are just defined by the rate of reaction, which is caused by dynamics.[14,15] Separating the mixed phases of Ni−B compounds is still a challenge. These amorphous defects and mixtures always influence the properties (conductivity, hardness, catalytical activity) of Ni−B compounds, which covered the intrinsic reasons for high performance and influence the judgment.[16] Therefore, synthesizing single phases of bulk Ni−B compounds is vital to uncover the more accurate structural parameters and to study the basic properties in the future. Besides, the excess B is always necessary in synthesis of transition metal borides (TMBs).[17−19] But it is difficult to detect the residual B in TMBs due to the B always being formed by amorphous.[20] So the effect of excess B in the synthesized process is still mysterious. Studying the influence in different proportions of starting materials and uncovering the form of residual B in TMBs is important.

Received: November 24, 2022
Accepted: February 21, 2023
Published: March 2, 2023

Together, the synthesis of Ni−B compounds needs to meet two conditions: one is enough energy to overcome the energy barrier, and the other is to control the experimental conditions to separate the mixed phases. The high pressure and high temperature (HPHT) method is an effective way to cross the energy barrier of Ni−B compounds in the synthesis process.[21−24] High pressure can promote the formation of strong covalent bonds in the structure, which is suitable to prepare Ni−B compounds. And controlling the pressure and temperature conditions can effectively control the growth rate of Ni−B compounds. Over the past decade, many single-phase bulk samples of TMBs are synthesized by HPHT.[17,25−27] However, single phase Ni−B compounds synthesized by HPHT are still rarely reported. Uncovering the growth mechanism of Ni−B compounds under HPHT is meaningful.

In this work, the chemical bonds (covalent bonds, ionic bonds, metal bonds) of Ni−B compounds are analyzed. The effect of pressure on the stability and the difficulties of synthesis in Ni−B compounds are studied by formation enthalpy and binding energy. Then, four single-phase bulk compounds of Ni_2B ($I4/mcm$), α-Ni_4B_3 ($Pnma$), β-Ni_4B_3 ($C2/c$), and NiB ($Cmcm$) are successfully synthesized by HPHT. The morphology of Ni−B compounds with different conditions is analyzed to understand the growth mechanism. The formation of residual B in samples is studied. The structures are refined to confirm the detailed information of space groups and lattice parameters. This work first uncovered the growth process of Ni−B compounds under HPHT, and it can be a guide for synthesizing strongly crystalline TMBs in the future.

2. THEORETICAL DETAILS

The first principle calculations of Ni_xB_y compounds (B ($R\bar{3}m$),[28] Ni ($Fm\bar{3}m$),[29] Ni_2B ($I4/mcm$),[30] α-Ni_4B_3 ($Pnma$),[31] β-Ni_4B_3 ($C2/c$),[14] and NiB ($Cmcm$)[32]) were executed with the Cambridge Serial Total Energy Package (CASTEP) program using density functional theory (DFT). The DFT exchange-correlation contribution is calculated using the Generalized-Gradient-Approximation (GGA) through the Perdew−Burke−Ernzerhof (PBE) functional. The electron−ion interaction was described by applying the projector augmented-wave method (PAW) with $3d^84s^2$ and $2s^22p^1$ as the valence electrons for Ni and B atoms, respectively. The cutoff energy of B and Ni was set to 250 and 400 eV, and the cutoff energy of other Ni_xB_y compounds was set to 500 eV. Correspondingly, the Brillouin zones were sampled with 3 × 3 × 3, 10 × 10 × 10, 4 × 4 × 5, 2 × 7 × 3, 3 × 4 × 3, and 7 × 3 × 7 k-points for geometry optimizations and electronic structure calculations. To explore the stability of the compounds under different pressures, the calculation of cohesive energy and formation enthalpy is crucial. The energy parameters are studied with the equation[30]

$$E_{coh}(Ni_xB_y) = \frac{E_{total}(Ni_xB_y, \text{cell}) - xnE_{iso}(Ni) - ynE_{iso}(B)}{n} \quad (1)$$

where $E_{coh}(Ni_xB_y)$ is the cohesive energy, $E_{total}(Ni_xB_y, \text{cell})$ is the total energy of the calculated Ni_xB_y conventional cell, $E_{iso}(Ni/B)$ is the total energy of an isolated Ni/B atom, and n is the total number of the Ni_xB_y units contained in the conventional cell. The formation enthalpy is studied with the equation[30]

$$\Delta H_r(Ni_xB_y) = E_{coh}(Ni_xB_y) - xE_{coh}(Ni) - yE_{coh}(B) \quad (2)$$

where $\Delta H_r(Ni_xB_y)$ is the formation enthalpy, and $E_{coh}(Ni/B)$ is the cohesive energy of Ni/B element per atom.

3. EXPERIMENT DETAILS

Ni_2B ($I4/mcm$), α-Ni_4B_3 ($Pnma$), β-Ni_4B_3 ($C2/c$), and NiB ($Cmcm$) were synthesized under HPHT. The raw materials were amorphous boron (99% in purity) and powdery nickel (99.99% in purity). Two kinds of powder were mixed in an agate mortar for more than 1.5 h at stoichiometric ratios of 2:1.2, 4:3.6, 4:3.6, and 1:1.2, respectively. It is necessary to increase the boron content to prevent the mixture phase. Then, the mixture was pressed into the pellets, which were placed in a capsule and treated in a 6 × 14,400 KN cubic anvil apparatus. The Ni_2B, α-Ni_4B_3, β-Ni_4B_3, and NiB were prepared at 5 GPa and under the temperature of 1400−1800, 1400, 2200, and 1000−1800 °C for 20, 20, 10, and 20 min, respectively. The synthesized block samples were ground in an agate mortar for 30 min, respectively. The phase analysis of the synthesized samples was evaluated by X-ray diffraction (XRD) with a Cu Kα X-ray beam (λ = 1.5418 Å) and the diffraction angle ranged from 20° to 80° and the scanning rate was 18°/min. The samples were ground 2 h by agate mortar, and the diffraction angle ranged from 25° to 65° and scanning rate was 2°/min. And then Rietveld structure refinements were implemented using the GSAS-II software package. In addition, the samples of fracture surfaces were detected by scanning electron microscopy (SEM, FEI Magellan 400 L). High-resolution transmission electron microscopy (HRTEM) images were obtained with a transmission electron microscope (TEM, JEM-2200FS).

4. RESULTS AND DISCUSSION

The Ni−B compounds have five common phases, Ni_3B ($Pnma$), Ni_2B ($I4/mcm$), α-Ni_4B_3 ($Pnma$), β-Ni_4B_3 ($C2/c$), and NiB ($Cmcm$), while the Ni_3B has a high content of metal Ni, which makes this compound more like solid-solution boron atoms in the Ni metals. Thus, the Ni_3B is not considered in this work. The skeletons of structures for Ni_2B ($I4/mcm$),[30] α-Ni_4B_3 ($Pnma$),[31] β-Ni_4B_3 ($C2/c$),[14] and NiB ($Cmcm$)[32] are shown in Figure 1. Ni atoms can form a three-dimensional (3D) skeleton in Ni_2B, due to the high Ni content (Figure 1a). This 3D metal skeleton also can generate an electronic channel and bring excellent conductivity (Figure 1a). The boron atoms in Ni_2B can form the special one-dimensional (1D) straight chain which is unusual in borides (Figure 1a). But the length of B−B bonds is 2.15 Å, which is comparable with metal bonds; therefore, the boron atoms in Ni_2B are only immersed in Ni metal skeletons. While the Ni 3D skeleton is destroyed by increasing the B content to form α-Ni_4B_3 ($Pnma$) (Figure 1b), α-Ni_4B_3 needs some isolated B atoms to connect the Ni substructure to form the 3D skeleton, and this 3D skeleton reserved some channels, which are inserted by zigzag B chains. This zigzag B chains are always formed by strong covalent bonds and can be found in TMBs[5]. Nevertheless, the allotrope of β-Ni_4B_3 ($C2/c$) can generate complex Ni atomic 3D skeleton, and with 1D B chains in parallel arrangement which likes the stepladder (Figure 1c). The high boron content NiB ($Cmcm$) can generate regular Ni 3D skeleton with oblate hexagonal channels, and the zigzag B chains are inserted in these channels (Figure 1d). So, according to the structures of Ni−B compounds, it can be speculated that Ni_2B and α-Ni_4B_3

https://doi.org/10.1021/acsomega.2c07523
ACS Omega 2023, 8, 9265−9274

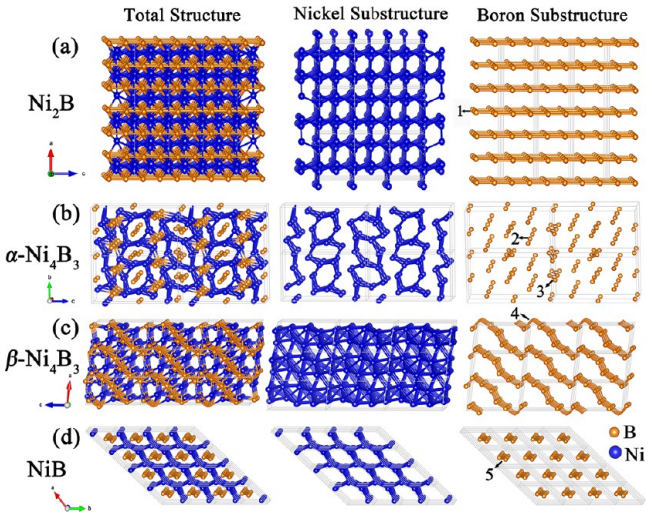

Figure 1. Structures of (a) Ni_2B, (b) α-Ni_4B_3, (c) β-Ni_4B_3, and (d) NiB compounds.

are major composed by Ni−Ni metal bonds and Ni−B ionic bonds, seldom B−B covalent bonds in α-Ni_4B_3. β-Ni_4B_3 and NiB have higher density of B−B covalent bonds and are composed by all of chemical bonds of Ni−Ni metal bonds, Ni−B ionic bonds and B−B covalent bonds.

To confirm the speculations about chemical bonds in Ni−B compounds, the electron localization functions (ELF) are shown in Figure 2. It is difficult to find the localized electrons

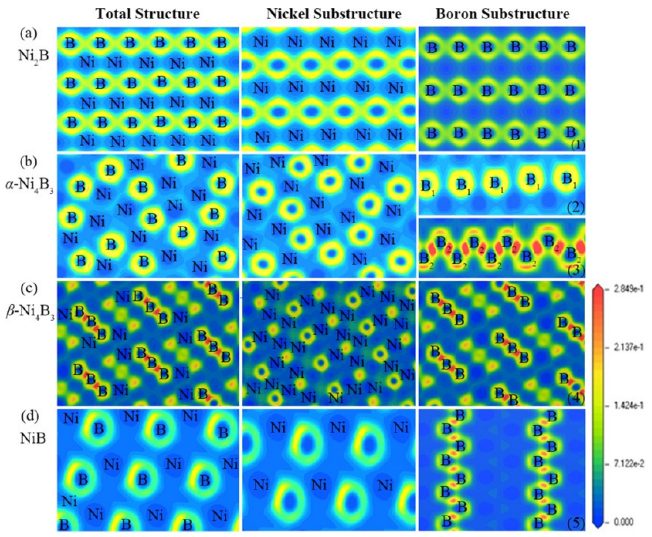

Figure 2. Electron localization functions (ELF) of compounds (a) Ni_2B, (b) α-Ni_4B_3, (c) β-Ni_4B_3, and (d) NiB.

in Ni_2B, which confirms that long B−B bonds (2.15 Å) are not the covalent bonds (Figure 2a). Moreover, the charge density difference of Ni_2B indicates the Ni atoms offer many electrons, and B atoms offer fewer electrons; both the offered electrons are full between Ni atoms and B atoms (Figure S1a); thus there are very weak ionic properties in Ni_2B. And DOS results indicate that all of the Ni−B compounds are conductors due to Ni 3d electrons and B 2p electrons having states at the Fermi level (Figure S2). Therefore, Ni_2B is mostly formed by metal bonds. The electrons are located between B atoms in zigzag chains and form covalent bonds in α-Ni_4B_3; between the isolated B atoms are not covalent bonds because no electrons are localized (Figure 2b). According to the charge density difference, Ni atoms lose many electrons, which transfer to B atoms (Figure S1b). Thus, Ni−B bonds belong to ionic bonds in α-Ni_4B_3. The stepladder-like B chain in β-Ni_4B_3 is combined by strong covalent bonds (Figure 2c). Ni atoms lose electrons and B atoms obtain electrons, which indicates that Ni−B bonds are ionic in the β-Ni_4B_3 (Figure S1c). Very strong covalent bonds are formed in B zigzag chains of NiB (Figure 2d); many electrons transfer from Ni atoms to B atoms and form ionic bonds (Figure S1d). According to the ELF, the charge density difference, and DOS, Ni_2B are mostly composed by metal bonds. There are some covalent bonds in α-Ni_4B_3, and most of the chemical bonds are metal bonds and ionic bonds. All of the covalent bonds, ionic bonds, and metal bonds are found in β-Ni_4B_3 and NiB, but NiB indicates stronger covalent bonds and ionic bonds than β-Ni_4B_3. So, β-Ni_4B_3 and NiB have high contents of the strongest covalent bonds and ionic bonds, which may need higher energy to synthesize these single phases.

To compare the stability of Ni−B compounds with different pressures is meaningful to choose the experimental conditions of pressure. The E_{coh} and the ΔH_r of Ni−B compounds with pressure range from 0−5 GPa were calculated. Figure 3 and

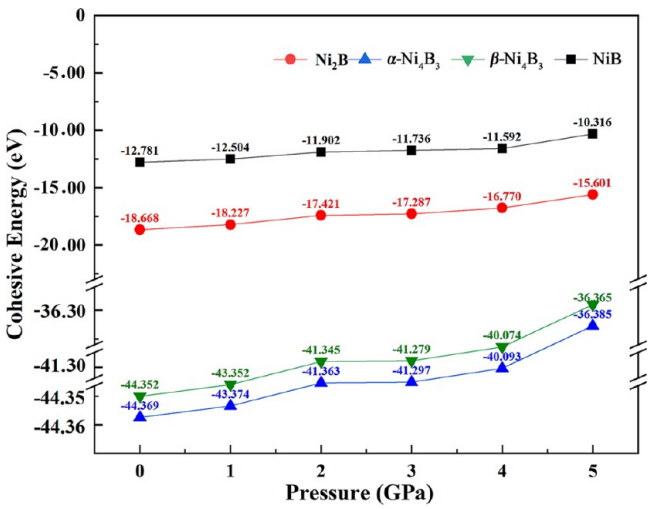

Figure 3. Cohesive energy of Ni−B compounds with pressure range of 0−5 GPa.

Table S1 indicate that Ni_2B, α-Ni_4B_3, β-Ni_4B_3, and NiB have negative E_{coh} and ΔH_r. It is consistent with the previous results of formation energy which demonstrate that all of these structures are stable.[31] Moreover, α-Ni_4B_3 is the most stable phase, followed by β-Ni_4B_3, Ni_2B, and NiB. The results indicate that it is difficult to decompose the α-Ni_4B_3 and β-Ni_4B_3, which means the synthesis of α-Ni_4B_3 and β-Ni_4B_3 need much more energy than Ni_2B and NiB. Higher pressure decreases the stability of Ni−B compounds with more positive E_{coh}, which indicates less energy is necessary to decompose Ni−B compounds with higher pressure. It is beneficial to synthesize Ni−B compounds under higher pressure.

The results above show that even though NiB has strong covalent bonds in the structure, synthesizing α-Ni_4B_3 and β-Ni_4B_3 needs much more energy than NiB and Ni_2B. And high pressure can promote synthesis of Ni−B compounds. So, almost the highest pressure (5 GPa) equipment is used, and

https://doi.org/10.1021/acsomega.2c07523
ACS Omega 2023, 8, 9265−9274

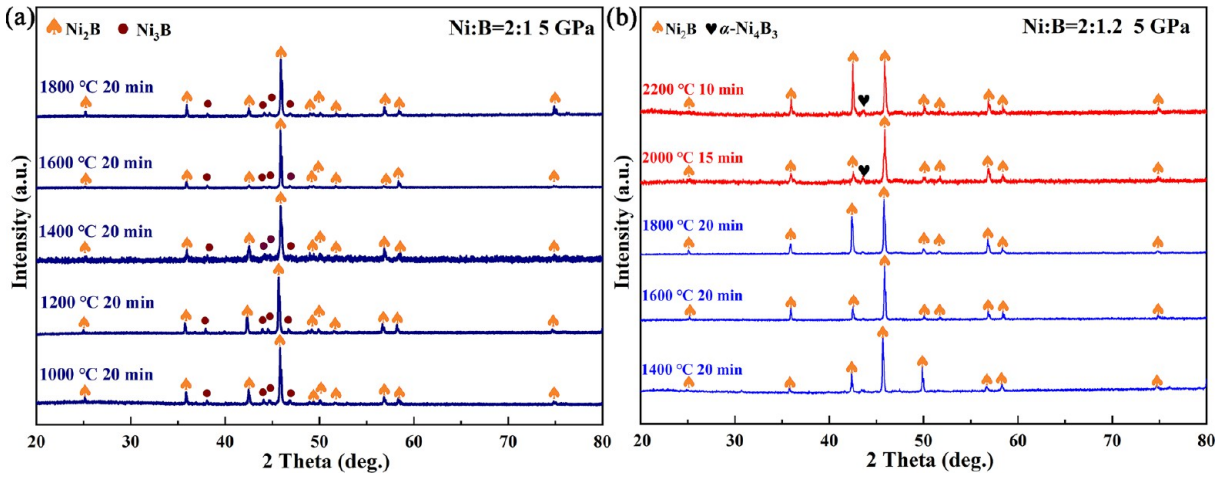

Figure 4. XRD patterns of Ni_2B at mole ratios of (a) Ni:B = 2:1 and (b) Ni:B = 2:1.2.

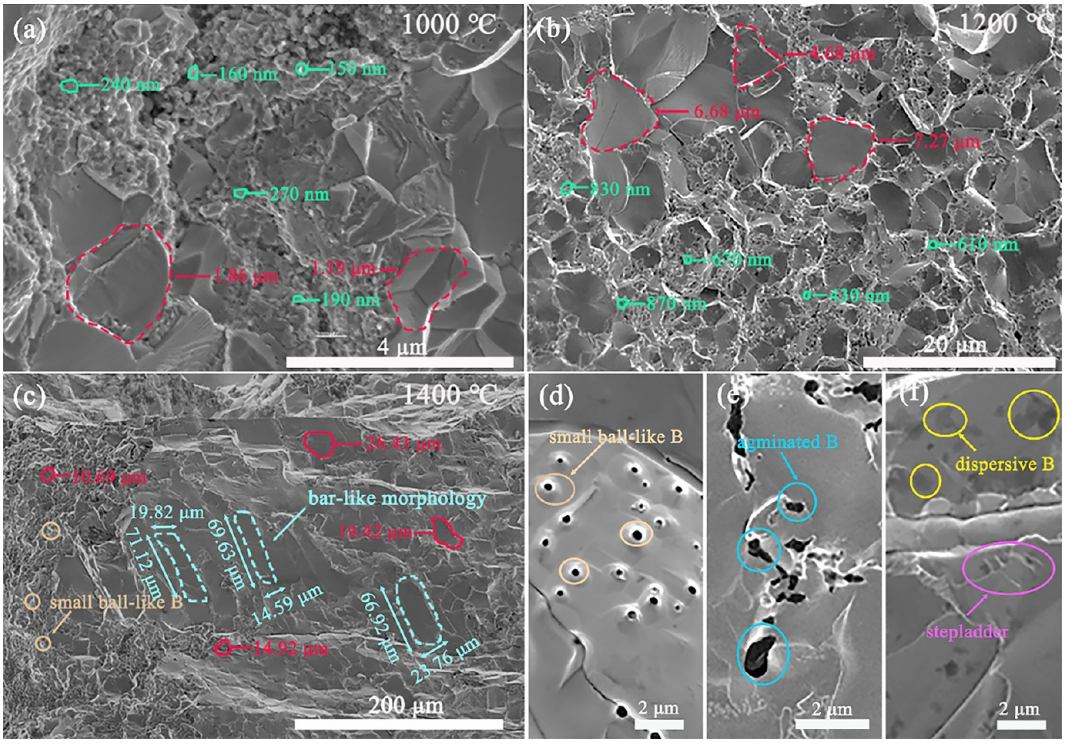

Figure 5. SEM results of samples with Ni:B = 2:1 under 5 GPa at (a) 1000 °C, (b) 1200 °C, and (c) 1400 °C. (d), (e), and (f) are the high magnification of the microscopic morphology at 1400 °C.

higher synthesized temperature is necessary for α-Ni_4B_3 and β-Ni_4B_3 than NiB and Ni_2B. However, according to the report of Zhou et al., all of the Ni−B compounds can generate spontaneous reaction by element Ni and element B at temperature range of 0−1200 K due to the Gibbs free energy of formations being negative.[14] Although the Gibbs free energy cannot completely define the reaction due to dynamic reasons, it also indicates that all of the Ni−B compounds may be easily formed to cause mixture in the sample. So accelerating the growth rate of the target product by high pressure and resisting the growth of a mixture at short synthesis time is important.

To synthesize the single phases of Ni−B compounds, high pressure of 5 GPa was chosen, and the temperature range from 1000 to 2200 °C was chosen, which is covered by the solid reaction temperature (1000−1500 °C) and the melting point of both Ni (1580 °C) and B (2425 °C) under 5 GPa.[33−35] In order to obtain microsize crystals, quick growth of the Ni−B compounds is needed; thus the temperatures lower than 1000 °C were not considered. And Ni_2B can be synthesized at the temperature higher than 1000 °C under 5 GPa (Figure 4a). And the sample has strong orientation at the (211) plane (46.14°). But the mixture of Ni_3B exists in the samples at the temperature range from 1000 to 1800 °C, which means higher temperature can not only accelerate the growth of Ni_2B and separate these two phases. This proportion of Ni:B = 2:1 can make the two products at 1000−1800 °C under 5 GPa. To obtain the single phase of Ni_2B, the proportion of Ni:B = 2:1.2 is used to resist growth of Ni_3B at 1400−2200 °C under 5 GPa. The XRD results show that single phase of Ni_2B is synthesized at 1400−1800 °C (Figure 4b), and the orientation

https://doi.org/10.1021/acsomega.2c07523
ACS Omega 2023, 8, 9265−9274

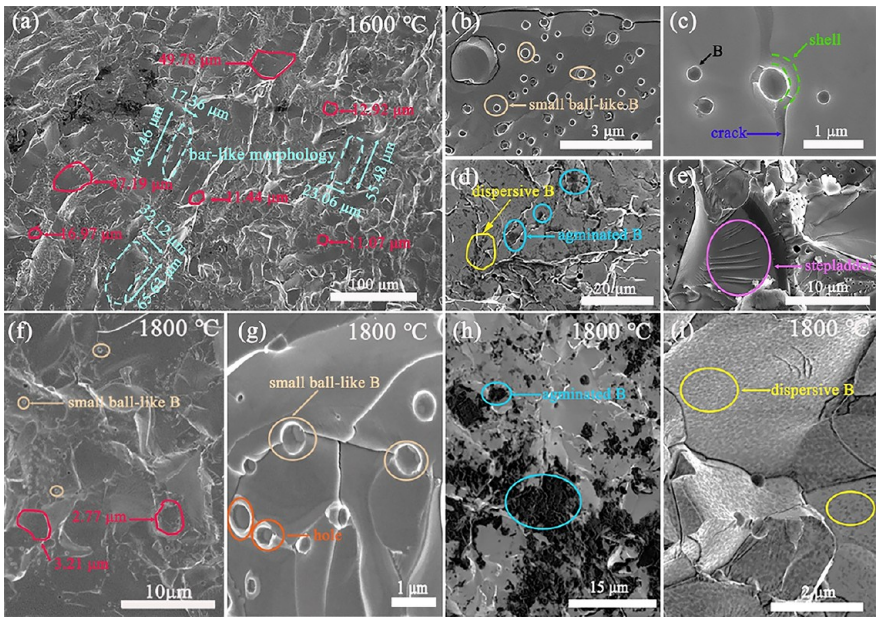

Figure 6. SEM results of samples with Ni:B = 2:1 at 1600−1800 °C under 5 GPa. (a) is the morphology at 1600 °C. (b), (c), (d), and (e) are the high magnification of the microscopic morphology at 1600 °C. (f), (g), (h), and (i) are the morphology at 1800 °C.

of (211) (46.14°) decreases with increasing temperature, which means the Ni_2B at the proportion of Ni:B = 2:1.2 has different morphology with the Ni_2B at the proportion of Ni:B = 2:1. But bits of α-Ni_4B_3 are from at the temperature higher than 2000 °C (Figure 4b), which indicates the higher B content can accelerate the α-Ni_4B_3 growth at high temperature (2000−2200 °C) or the Ni_2B may react with B to form α-Ni_4B_3 at 2000−2200 °C; it is difficult to know. So, the reaction at the Ni:B = 2:1.2 and temperature of 1400−1800 °C under 5 GPa is

$$2Ni + 1.2B \rightarrow Ni_2B + 1/5B \quad (3)$$

A bit more B is necessary which may be for dynamic reasons (will discuss below), and many before works confirmed that excess boron is preferred to synthesize a single phase of TMBs.[17−19] While the additional boron always forms amorphous structures in the samples, which cannot be tested by XRD. Thus, actually a bit of amorphous boron is mixed in the samples synthesized at Ni:B = 2:1.2 and temperature of 1400−1800 °C under 5 GPa. So according to reaction 4, the reactions of Ni:B = 2:1 at 1000−1800 °C under 5 GPa can be speculated that

$$2Ni + 1B \rightarrow 2/5Ni_2B + 2/25B + 2/5Ni_3B + 3/25B \quad (4)$$

Therefore, even at the stoichiometric ratio, the additional B is needed to grow the Ni_2B and Ni_3B.

Uncovering the morphology of samples is important to understand the dynamic mechanism of Ni_2B growth. The SEM results of samples with Ni:B = 2:1 at 1000−1800 °C under 5 GPa are shown in Figure 5 and Figure 6. The nanoparticles with 100−300 nm and microsize particles (1−4 μm) are found at the fracture surface of sample (1000 °C, Figure 5a), meaning that the sample is at the stage of crystal growth which is after nucleation. Both the nanosize and microsize of particles in one sample also confirm that HPHT can quickly grow the particles after the stages of diffusion and nucleation. Thus, if nucleation is finished, it will quickly grow to microsize under HPHT. But the lower diffusion of the solid reaction restricts the nucleation because the nucleation has different rates at different parts, which makes both nanosize and microsize particles in the sample. The content of nanoparticles in the samples decreases with increasing temperature to 1200 °C (Figure 5b). The size of nanoparticles increased to about 300−900 nm in the sample (1200 °C), and the size of microparticles grew to 3−12 μm. Almost no nanoparticles are found in the samples at 1400 °C (Figure 5c). The size of microparticles increased to 5−30 μm, and except for the particle morphology, some bar-like morphology is formed in the sample. The large area of the flat surface of bar-like crystals may be the (211) crystal plane of Ni_2B, which can make strong orientation and is consistent with XRD results (Figure 4a). In general, the excess B is difficult to find in the TMBs when the content of excess B is small.[36] The excess B is immersed in nanoparticles or Ni_2B particles in the samples of 1000 and 1200 °C, but the excess B is exposed by high temperature accelerating the diffusion in the sample of 1400 °C. Three forms of B in the sample (1400 °C) are found. First is the small ball-like B (Figure 5d), which is separated out from Ni_2B crystal, and this small ball may not an entire B, but may also be covered by Ni_2B shell (discuss below). The second form of B in the sample is agminated B which is at the grain boundary of Ni_2B (Figure 5e). This B may be the residual B which is not covered by Ni and also incompletely reacts with Ni. The third form of B is the dispersive B (Figure 5f), which may be caused by a special proportion of Ni and B in a local part of the sample when the temperature sharply decreases to room temperature, and it is like the eutectic phase. The B small ball is the major form in the sample because high temperature separates out much of B small balls in the sample of 1600 °C (Figure 6a). This is because the high temperature of 1600 °C under 5 GPa can make the Ni melt at the start and accelerate the diffusion of Ni to cover B, finally generating much of the B small balls. The content of the bar-like crystals increases with the size about 20 μm in thickness and 80 μm in length (Figure 6a). The shell of small ball-like B is shown in Figure 6b, and the crack can be formed on both sides of small ball-like B, due

https://doi.org/10.1021/acsomega.2c07523
ACS Omega 2023, 8, 9265−9274

to the strong mechanical properties and different thermal expansion coefficient of B and Ni_2B (Figure 6c).[37−40] The dispersive B and agminated B also can be found in sample of 1600 °C (Figure 6d), and the growth step can be found in the microsize particles (Figure 6e). The morphology of Ni_2B in the sample of 1800 °C is close to the sample of 1600 °C (Figure 6f). Except for the small ball-like B (Figure 6g), the dispersive B and agminated B are easily found in the sample of 1800 °C (Figure 6h,i), which may be because quenching from higher temperature is more suitable to capture the eutectic phase and higher temperature can cause the B aggregation. It is a pity that it is difficult to determine the mixture of Ni_3B in the samples due to the reduced content of Ni_3B and Ni_3B and Ni_2B have the same morphology.

Why the small ball-like B can be formed in Ni−B compounds is confusing. Figure 7 indicates the diffusion of Ni and B caused by HPHT, and also can explain the reason for small ball-like B in samples. The diffusion coefficient of B is much lower than Ni, which will generate the Ni diffusion faster than B, then separate B and cover the B.[41−43] The nucleon and Ni_2B phases are formed at the interface of Ni and B. Nevertheless, the Ni_2B will impede the Ni diffusion to cross itself with increasing thickness of Ni_2B, which will stop the reaction between Ni and B. Finally, Ni_2B forms a shell (Figure 6c) and leaves the residual B in it. This is also the reason that a bit more B is necessary to synthesize a single phase of TMBs. And the small ball-like B with or without the Ni_2B shell can be separated out at high temperature such as in the sample with 1400 °C (Figure 6d).

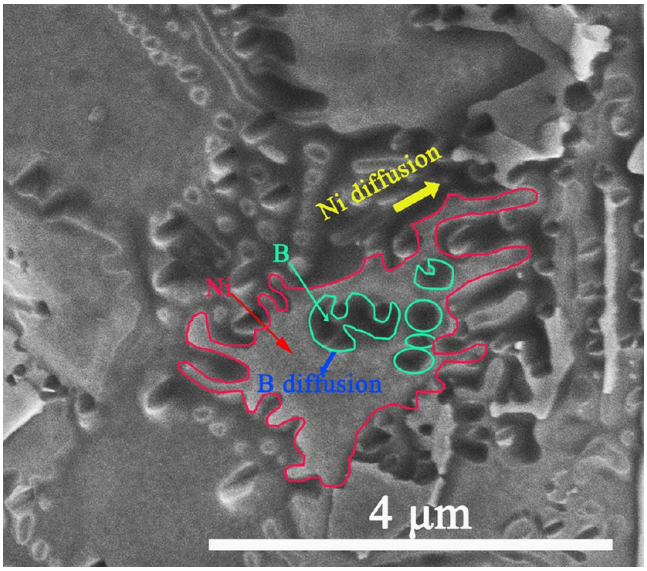

Figure 7. Morphololgy of diffusion of Ni and B.

With higher B content of Ni:B = 2:1.2, also the nanosize of Ni_2B particles and microsize Ni_2B particles are found in Ni:B = 2:1.2 at temperature of 1400 °C under 5 GPa (Figure S3a,b). Both the nanosize of Ni_2B particles (200 nm−700 nm) and microsize Ni_2B particles (20 μm−80 μm) are bigger than Ni:B = 2:1 in the same temperature. These results indicate that the growth rate of Ni_2B increases with increasing the B content. The intrinsic reason is that high B content supples the weakness of low diffusion coefficient of B. The small ball-like B, dispersive B, and agminated B are all found in the samples with higher temperature of 1600−2200 °C (Figure S3c−j). But the bar-like morphology is not found in the samples with Ni:B = 2:1.2; it is consistent with XRD results, which have no orientation in the (211) crystal plane (Figure 4b). Moreover, the grain size of Ni_2B is increased with higher temperature before 1800 °C; then the grain size decreases with a higher temperature over 1800 °C (Figure S3). This indicates higher temperature over 1800 °C decreases the growth rate of Ni_2B, which may be because the Ni_2B is metastable under these high temperature, and the mixture of α-Ni_4B_3 is formed (Figure 4b).

The above results indicate the excess boron is needed to synthesize Ni−B compounds. This phenomenon is also found in synthesizing the two phases of α-Ni_4B_3 and β-Ni_4B_3. The stoichiometric ratio of Ni:B = 4:3 can only obtain the samples of α-Ni_4B_3 with mixture of Ni_2B at temperature range from 1000 to 2200 °C (Figure 8a), and the excess B of Ni:B = 4:3.6 can impede the growth of Ni_2B (Figure 8b). But NiB is formed as the mixture in α-Ni_4B_3 with low temperature of 1000 °C (Figure 8b). Even the NiB is the major phase of sample (Figure 8b, 1000 °C), while the content of NiB decreases with a high temperature of 1200 °C, and α-Ni_4B_3 becomes the major phase. The single phase of α-Ni_4B_3 is synthesized at 1400 °C. Thus, synthesizing α-Ni_4B_3 requires much more energy than NiB. However, the α-Ni_4B_3 and β-Ni_4B_3 mixture is

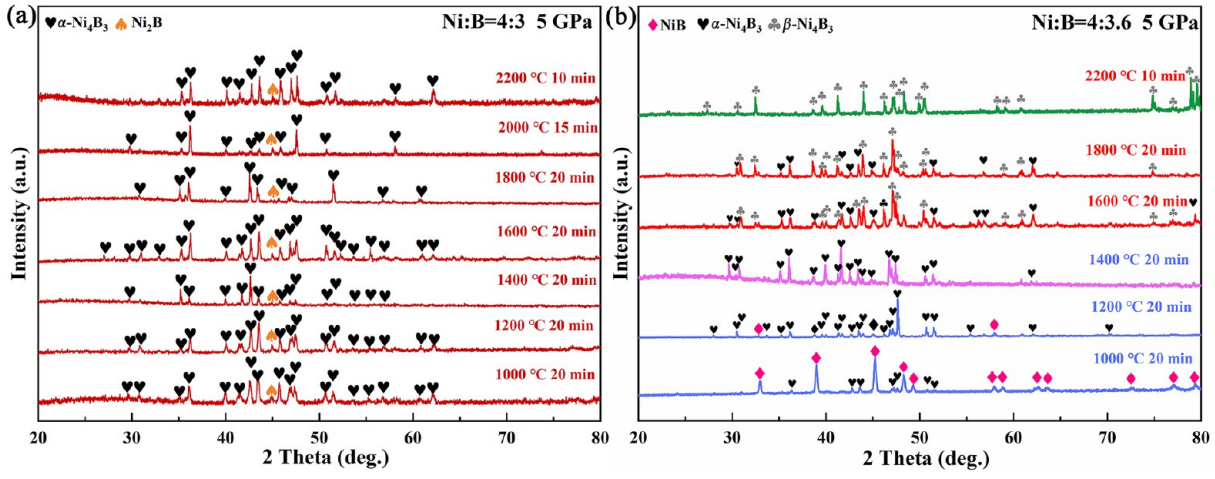

Figure 8. XRD patterns of Ni_4B_3 at mole ratios of (a) Ni:B = 4:3 and (b) Ni:B = 4:3.6.

https://doi.org/10.1021/acsomega.2c07523
ACS Omega 2023, 8, 9265−9274

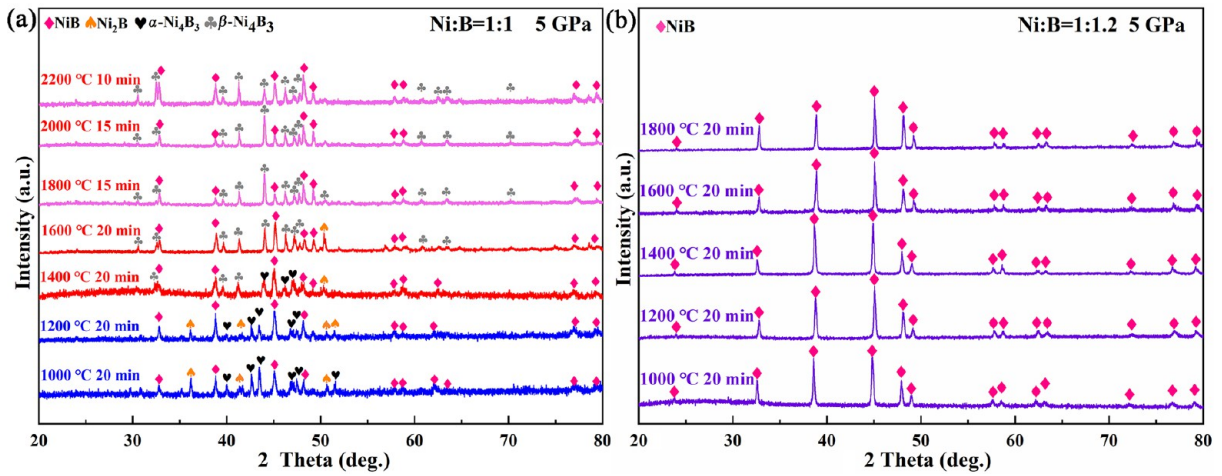

Figure 9. XRD patterns of NiB at mole ratios of (a) Ni:B = 1:1 and (b) Ni:B = 1:1.2.

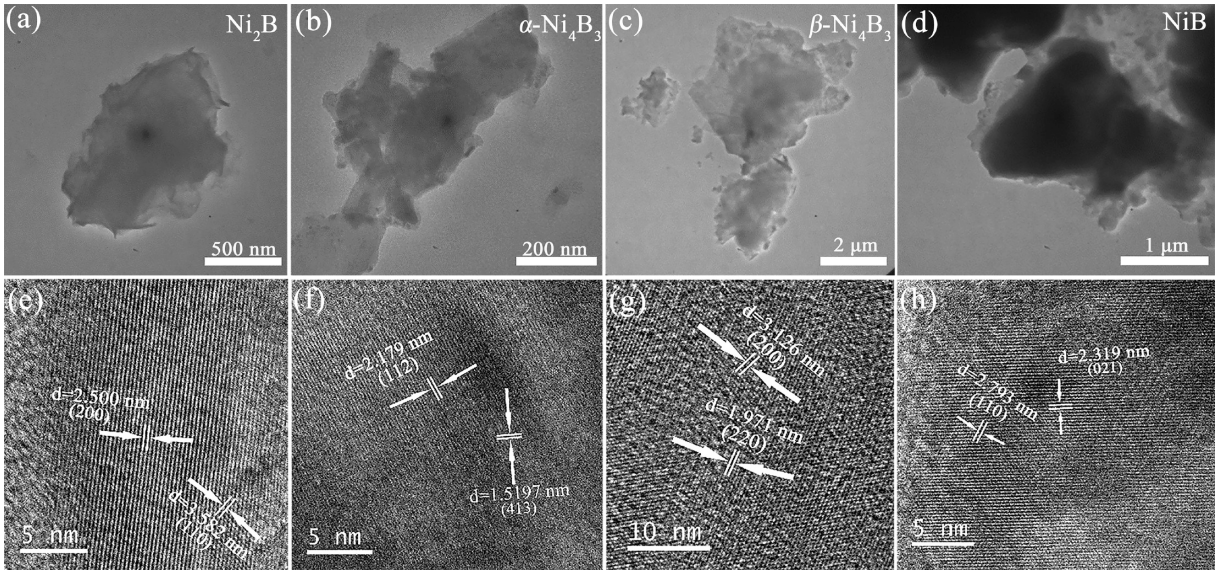

Figure 10. TEM and HRTEM images of Ni−B compounds: (a) and (e) are the morphology of Ni_2B; (b) and (f) are the morphology of α-Ni_4B_3; (c) and (g) are the morphology of β-Ni_4B_3; (d) and (h) are the morphology of NiB.

synthesized with a higher temperature of 1600 °C. Moreover, the content of α-Ni_4B_3 decreases with increasing the temperature. The single phase of β-Ni_4B_3 is synthesized at a high temperature of 2200 °C. Therefore, it is confirmed that β-Ni_4B_3 is the high-temperature phase and α-Ni_4B_3 is the low-temperature phase of Ni_4B_3, and α-Ni_4B_3 is more stable than β-Ni_4B_3. According to reaction 5, producing Ni_2B needs about 1/5 excess B, so the reaction of Ni:B = 4:3, Ni:B = 4:3.6 (1400 °C), and Ni:B = 4:3.6 (2200 °C) can be speculated as

$$4Ni + 3B \rightarrow 2/3\alpha - Ni_4B_3 + 1/5B + 2/3Ni_2B + 2/15B \quad (5)$$

$$4Ni + 3.6B \rightarrow \alpha\text{-}Ni_4B_3 + 1/2B + 1/10B \quad (6)$$

$$4Ni + 3.6B \rightarrow \beta\text{-}Ni_4B_3 + 1/2B + 1/10B \quad (7)$$

Producing Ni_4B_3 needs about 1/2 excess B.

At the stoichiometric ratio of Ni:B = 1:1 (1000−2200 °C, 5 GPa), the major phase is NiB, and the mixture is Ni_4B_3, due to the proportion of 1:1 being close to 4:3 (Figure 9a). The mixture of the low-temperature phase of α-Ni_4B_3 and Ni_2B exists in 1000 and 1200 °C, and the high-temperature phase of β-Ni_4B_3 is at 1400−2200 °C. The single phases of NiB are synthesized at Ni:B = 1:1.2 (1000−1800 °C, 5 GPa), shown in Figure 9b. The reaction of Ni:B = 1:1 and Ni:B = 1:1.2 can be speculated as

$$Ni + B \rightarrow 1/7NiB + 1/35B + 1/7\alpha - Ni_4B_3 + 3/70B + 1/7Ni_2B + 1/35B + 13/70B \quad (8)$$

$$Ni + B \rightarrow 1/5NiB + 1/25B + 1/5\beta\text{-}Ni_4B_3 + 1/10B + 3/50B \quad (9)$$

$$Ni + 1.2B \rightarrow NiB + 1/5B \quad (10)$$

SEM results also indicate that the growth process of α-Ni_4B_3, β-Ni_4B_3, and NiB is very close to Ni_2B. The samples are also composed by nanosize particles and microsize particles at low temperature (Figures S4−S7). And it is easy to find the growth step in microsize particles, and the B also have three forms of small ball-like B, dispersive B, and agminated B in the samples (Figures S4−S7). So, the Ni_2B, α-Ni_4B_3, β-Ni_4B_3, and NiB are

https://doi.org/10.1021/acsomega.2c07523
ACS Omega 2023, 8, 9265−9274

synthesized, even though a bit of boron in the samples, but it will not dramatically influence the properties of samples,[25,44,45] because the major form of B is small ball-like B, which is at local position and will influence the local properties. If the major form of B is dispersive B, it will exhibit distinct properties. All the samples are well crystallized with more than 20 μm; the single phase of microsize Ni−B compounds has rarely been reported before. To further confirm the crystal structure and the lattices of Ni−B compounds, the Rietveld refinements are performed. The results are shown in Figure S8 and Table S2. And all of the space, lattice parameters, and atomic positions are consistent with previous reports.[46−48] The lattices of Ni−B compounds are also confirmed by HRTEM in Figure 10.

According to the above results, the growth process of Ni−B compounds is speculated (Figure 11): (1) the different

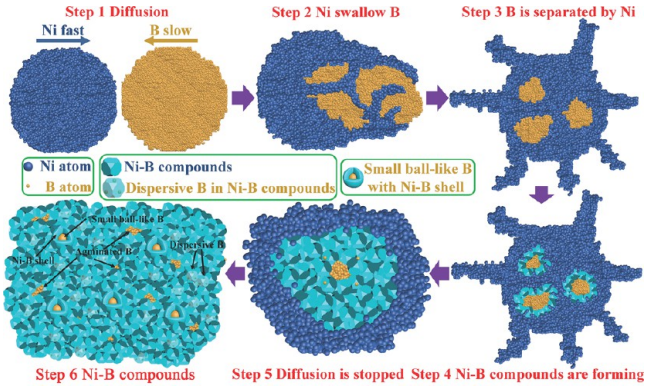

Figure 11. Speculating growth process of Ni−B compounds.

diffusion coefficients of Ni and B make the B covered by Ni and cause residual small ball-like B in the samples, and require excessive B. (2) Ni and B do not distribute homogeneously making different growth rates in different parts of samples, and cause both nanosize and microsize particles at low temperature. (3) High temperature can not only generate grains to grow to microsize particles, but also separate out the small ball-like B (covered with Ni−B compounds shell). (4) The residual B has three forms of small ball-like B, dispersive B, and agminated B, and the small ball-like B is the major form.

5. CONCLUSION

In summary, the single phase of Ni_2B, α-Ni_4B_3, β-Ni_4B_3, and NiB are synthesized by HPHT, and these structures are confirmed by Rietveld refinement. Although NiB has the strongest covalent bonds and highest Gibbs free energy in the Ni−B compounds, synthesizing α-Ni_4B_3 and β-Ni_4B_3 needs more energy than Ni_2B and NiB. Because of different diffusion ability between Ni and B, the growth mechanism of Ni covering B to form Ni−B compounds is found, which also makes the excess B necessary in synthesizing Ni−B compounds. The residual B in the structure has three forms of small ball-like B, dispersive B, and agminated B are uncovered. Generating homogeneous distribution of start materials and increasing the interdiffusion between TM and B are two keys to synthesize highly crystalline and pure samples by HPHT. This work uncovers the growth process of Ni−B compounds and finds the forms of residual B in Ni−B compounds. It is significant for synthesizing highly crystalline TMBs in the future.

ASSOCIATED CONTENT

Supporting Information

The Supporting Information is available free of charge at https://pubs.acs.org/doi/10.1021/acsomega.2c07523.

Charge density difference; density of states; SEM results of different experimental conditions; enthalpy of formation at 0−5 GPa; Rietveld refine results; Crystal data and structure refinements (PDF)

AUTHOR INFORMATION

Corresponding Authors

Qiang Tao − *State Key Laboratory of Superhard Materials, College of Physics, Jilin University, Changchun 130012, People's Republic of China;* orcid.org/0000-0002-6357-5552; Email: qiangtao@jlu.edu.cn

Shushan Dong − *State Key Laboratory of Superhard Materials, College of Physics, Jilin University, Changchun 130012, People's Republic of China*; Email: dongss@jlu.edu.cn

Pinwen Zhu − *State Key Laboratory of Superhard Materials, College of Physics, Jilin University, Changchun 130012, People's Republic of China*; Email: zhupw@jlu.edu.cn

Authors

Guiqian Sun − *State Key Laboratory of Superhard Materials, College of Physics, Jilin University, Changchun 130012, People's Republic of China*

Xingbin Zhao − *Institute of High Pressure Physics, School of Physical Science and Technology, Ningbo University, Ningbo 315211, People's Republic of China*

Lu Chen − *State Key Laboratory of Superhard Materials, College of Physics, Jilin University, Changchun 130012, People's Republic of China*

Yubo Fu − *State Key Laboratory of Superhard Materials, College of Physics, Jilin University, Changchun 130012, People's Republic of China*

Wei Zhao − *State Key Laboratory of Superhard Materials, College of Physics, Jilin University, Changchun 130012, People's Republic of China*

Meiyan Ye − *State Key Laboratory of Superhard Materials, College of Physics, Jilin University, Changchun 130012, People's Republic of China*

Fei Wang − *State Key Laboratory of Superhard Materials, College of Physics, Jilin University, Changchun 130012, People's Republic of China*

Complete contact information is available at: https://pubs.acs.org/10.1021/acsomega.2c07523

Notes

The authors declare no competing financial interest.

ACKNOWLEDGMENTS

This work was supported by the National Natural Science Foundation of China (under grant Nos. 11904119, 11974131), China postdoctoral Science Foundation (No. 2016M601374), the National Key R&D Program of China (2018YFA0703400), Henan Provincial Department and Technology of China (under grant No. 211110230500).

REFERENCES

(1) Başarır, E.; Özkan, G.; Özkan, G. Synthesis of nickel boride and investigation of availability as an additive in the molten carbonate fuel cell anode material. *Int. J. Energy Res.* **2022**, *46*, 10088−10098.

(2) Levine, J. B.; Tolbert, S. H.; Kaner, R. B. Advancements in the Search for Superhard Ultra-Incompressible Metal Borides. *Adv. Funct. Mater.* **2009**, *19*, 3519−3533.

(3) Feng, Y.; Li, Y.; Yuan, H. Effects of amorphous NiB on electrochemical characteristics of MgNi alloy. *J. Alloys Compd.* **2009**, *468*, 575−580.

(4) Xu, C.; He, D.; Wang, H.; Wang, W.; Tang, M.; Wang, P. Synthesis of novel superhard materials under ultrahigh pressure. *Chin. Sci. Bull.* **2014**, *59*, 5251−5257.

(5) Carenco, S.; Portehault, D.; Boissiere, C.; Mezailles, N.; Sanchez, C. Nanoscaled metal borides and phosphides: recent developments and perspectives. *Chem. Rev.* **2013**, *113*, 7981−8065.

(6) Gu, Q.; Krauss, G.; Steurer, W. Transition Metal Borides: Superhard versus Ultra-incompressible. *Adv. Mater.* **2008**, *20*, 3620−3626.

(7) Shahbazi, M.; Cathey, H.; Danilova, N.; Mackinnon, I. D. R. Single Step Process for Crystalline Ni-B Compounds. *Materials* **2018**, *11*, 1259.

(8) Gouget, G.; Beaunier, P.; Portehault, D.; Sanchez, C. New route toward nanosized crystalline metal borides with tuneable stoichiometry and variable morphologies. *Faraday Discuss.* **2016**, *191*, 511−525.

(9) Le Godec, Y.; Courac, A. In Situ High-Pressure Synthesis of New Outstanding Light-Element Materials under Industrial P-T Range. *Materials* **2021**, *14*, 4245.

(10) Glavee, G. N.; Klabunde, K. J.; Sorensen, C. M.; Hadjipanayis, G. C. Borohydride reduction of nickel and copper ions in aqueous and nonaqueous media. Controllable chemistry leading to nanoscale metal and metal boride particles. *Langmuir* **1994**, *10*, 4726−4730.

(11) Corrias, A.; Ennas, G.; Musinu, A.; Marongiu, G.; Paschina, G. Amorphous transition metal-boron ultrafine particles prepared by chemical methods. *Chem. Mater.* **1993**, *5*, 1722−1726.

(12) Caputo, R.; Guzzetta, F.; Angerhofer, A. Room-temperature synthesis of nickel borides via decomposition of $NaBH_4$ promoted by nickel bromide. *Inorg. Chem.* **2010**, *49*, 8756−8762.

(13) Liaw, B. J.; Chiang, S. J.; Tsai, C. H.; Chen, Y. Z. Preparation and catalysis of polymer-stabilized NiB catalysts on hydrogenation of carbonyl and olefinic groups. *Appl. Catal., A* **2005**, *284*, 239−246.

(14) Kong, Y.; Xiong, W.; Guo, H.; Sun, W.; Du, Y.; Zhou, Y. Elastic and thermodynamic properties of the Ni−B system studied by first-principles calculations and experimental measurements. *Calphad.* **2010**, *34*, 245−251.

(15) Sun, W. H.; Du, Y.; Kong, Y.; Xu, H. H.; Xiong, W.; Liu, S. H. Reassessment of the Ni-B system supported by key experiments and first-principles calculation. *Int. J. Mater. Res.* **2009**, *100*, 59−67.

(16) Mukhanov, V. A.; Kurakevych, O. O.; Solozhenko, V. L. Thermodynamic model of hardness: Particular case of boron-rich solids. *J. Superhard Mater.* **2010**, *32*, 167−176.

(17) Tian, R.; Zhao, S.; Li, J.; Chen, Z.; Peng, W.; He, Y.; Zhang, L.; Yan, S.; Wu, L.; Ahuja, R.; Gou, H. Pressure-promoted highly-ordered Fe-doped-Ni_2B for effective oxygen evolution reaction and overall water splitting. *J. Mater. Chem. A* **2021**, *9*, 6469−6475.

(18) Zhao, X.; Liu, X.; Lin, F.; Liu, W.; Su, W. A new route for the synthesis of boronrich rare-earth boride NdB_6 under high pressure and high temperature. *J. Alloys Compd.* **1997**, *249*, 247−250.

(19) Petermuller, B.; Neun, C.; Wurst, K.; Bayarjargal, L.; Zimmer, D.; Morgenroth, W.; Avalos-Borja, M.; Becerril-Juarez, I. G.; Muhlbauer, M. J.; Winkler, B.; Huppertz, H. High-Pressure Synthesis of β-Ir_4B_5 and Determination of the Compressibility of Various Iridium Borides. *Inorg. Chem.* **2018**, *57*, 10341−10351.

(20) Le Godec, Y.; Courac, A.; Solozhenko, V. L. High-pressure synthesis of superhard and ultrahard materials. *J. Appl. Phys.* **2019**, *126*, 151102.

(21) Zhang, L.; Cheng, Y.; Lei, L.; Wang, X.; Hu, Q.; Wang, Q.; Ohfuji, H.; Kojima, Y.; Zhang, Q.; Zeng, Z.; Peng, F.; Kou, H.; He, D.; Irifune, T. High-Pressure Synthesis of CeOCl Crystals and Investigation of Their Photoluminescence and Compressibility Properties. *Cryst. Growth Des.* **2018**, *18*, 1843−1847.

(22) Shatskiy, A.; Borzdov, Y. M.; Yamazaki, D.; Litasov, K. D.; Katsura, T.; Palyanov, Y. N. Aluminum Nitride Crystal Growth from an Al−N System at 6.0 GPa and 1800 °C. *Cryst. Growth Des* **2010**, *10*, 2563−2570.

(23) Lei, L.; He, D. Synthesis of GaN crystals through solid-state metathesis reaction under high pressure. *Cryst. Growth Des.* **2009**, *9*, 1264−1266.

(24) Antlauf, M.; Taniguchi, T.; Wagler, J.; Schwarz, M. R.; Kroke, E. Synthesis of Large Rare Earth Element Germanate Pyrochlore Single Crystals at High Pressure. *Cryst. Growth Des.* **2019**, *19*, 5538−5543.

(25) Zhao, X.; Li, L.; Bao, K.; Zhu, P.; Tao, Q.; Ma, S.; Cui, T. Insight the effect of rigid boron chain substructure on mechanical, magnetic and electrical properties of β-FeB. *J. Alloys Compd.* **2022**, *896*, 162767.

(26) Wang, Y.; Guang, X.; Pan, M. Mechanochemical synthesis and high-capacity performances of transition-metal borides as aqueous anode materials. *Chin. Sci. Bull.* **2012**, *57*, 4225−4228.

(27) Ge, Y.; Bao, K.; Ma, T.; Zhang, J.; Zhou, C.; Ma, S.; Tao, Q.; Zhu, P.; Cui, T. Revealing the Unusual Boron-Pinned Layered Substructure in Superconducting Hard Molybdenum Semiboride. *ACS Omega* **2021**, *6*, 21436−21443.

(28) Fujimori, M.; Nakata, T.; Nakayama, T.; Nishibori, E.; Kimura, K.; Takata, M.; Sakata, M. Peculiar covalent bonds in alpha-rhombohedral boron. *Phys. Rev. Lett.* **1999**, *82*, 4452−4455.

(29) Connétable, D.; Thomas, O. First-principles study of the structural, electronic, vibrational, and elastic properties of orthorhombic NiSi. *Phys.Rev.B* **2009**, *79*, No. 094101.

(30) Zhou, C. T.; Xing, J. D.; Xiao, B.; Feng, J.; Xie, X. J.; Chen, Y. H. First principles study on the structural properties and electronic structure of X_2B (X = Cr, Mn, Fe, Co, Ni, Mo and W) compounds. *Comput. Mater. Sci.* **2009**, *44*, 1056−1064.

(31) Wang, K.; Du, D.; Chang, B.; Hong, Y.; Ju, J.; Sun, S.; Fu, H. Mechanical Properties, Electronic Structures, and Debye Temperature of Ni_xB_y Compounds Obtained by the First Principles Calculations. *Crystals* **2018**, *8*, 451.

(32) Zhou, Y.; Xiang, H.; Feng, Z.; Li, Z.; Pharr, G. Electronic Structure and Mechanical Properties of NiB: A Promising Interphase Material for Future UHTCf/UHTC Composites. *J. Am. Ceram. Soc.* **2016**, *99*, 2110−2119.

(33) Wang, Z.; Lazor, P.; Saxena, S. A simple model for assessing the high pressure melting of metals: nickel, aluminum and platinum. *Physica B: Condensed Matter* **2001**, *293*, 408−416.

(34) Boccato, S.; Torchio, R.; Kantor, I.; Morard, G.; Anzellini, S.; Giampaoli, R.; Briggs, R.; Smareglia, A.; Irifune, T.; Pascarelli, S. The Melting Curve of Nickel Up to 100 GPa Explored by XAS. *J. Geophys. Res. Solid Earth* **2017**, *122*, 9921−9930.

(35) Solozhenko, V. L.; Kurakevych, O. O. Equilibrium p-T phase diagram of boron: experimental study and thermodynamic analysis. *Sci. Rep.* **2013**, *3*, 2351.

(36) Dinh, K. N.; Liang, Q.; Du, C.-F.; Zhao, J.; Tok, A. I. Y.; Mao, H.; Yan, Q. Nanostructured metallic transition metal carbides, nitrides, phosphides, and borides for energy storage and conversion. *Nano Today* **2019**, *25*, 99−121.

(37) Yu, L. X.; Sun, Y. R.; Sun, W. R.; Zhang, W. H.; Liu, F.; Xin, X.; Qi, F.; Jia, D.; Sun, X. F.; Guo, S. R.; Hu, Z. Q. Effect of B on microstructure and properties of low thermal expansion superalloy. *J. Mater. Sci. Technol.* **2013**, *29*, 1470−1477.

(38) Nazarian-Samani, M.; Kamali, A. R.; Nazarian-Samani, M.; Mobarra, R.; Naserifar, S. Thermokinetic study on the phase evolution of mechanically alloyed Ni−B powders. *J. Therm. Anal. Calorim.* **2012**, *107*, 265−269.

(39) Stepanova, A.; Lad'yanov, V.; Nurgayanov, R.; Chudinov, V. Structural model of the Ni_2B amorphous alloy from the data of molecular dynamics simulation. *Glass Phys. Chem.* **2000**, *26*, 342−345.

(40) Hu, X.; Björkman, T.; Lipsanen, H.; Sun, L.; Krasheninnikov, A. V. Solubility of Boron, Carbon, and Nitrogen in Transition Metals:

https://doi.org/10.1021/acsomega.2c07523
ACS Omega 2023, 8, 9265−9274

Getting Insight into Trends from First-Principles Calculations. *J. Phys. Chem. Lett.* **2015**, *6*, 3263−3268.
(41) Keddam, M.; Jurci, P. Assessment of Boron Diffusivities in Nickel Borides by Two Mathematical Approaches. *Materials* **2022**, *15*, 555.
(42) Heinz, P.; Volek, A.; Singer, R. F.; Dinkel, M.; Pyczak, F.; Göken, M.; Ott, M.; Affeldt, E.; Vossberg, A. Diffusion brazing of single crystalline nickel base superalloys using boron free nickel base braze alloys. *Defect. Diffus. Forum.* **2008**, *273*, 294−299.
(43) Makuch, N. Nanomechanical properties and fracture toughness of hard ceramic layer produced by gas boriding of Inconel 600 alloy. *T. Nonferr. Metal. Soc.* **2020**, *30*, 428−448.
(44) Zhao, X.; Zhou, C.; Bao, K.; Zhu, P.; Ma, S.; Tao, Q.; Cui, T. Synthesis, Characterization, and First-Principles Analysis of the MAB-Like Ternary Transition-Metal Boride $Fe(MoB)_2$. *Inorg. Chem.* **2022**, *61*, 11046−11056.
(45) Zuo, Y.; Liu, Z.; Zhao, W.; Liu, Y.; Gai, X.; Han, D.; Wang, X.; Dong, S.; Tao, Q.; Zhu, P. Enhanced hardness and conductivity motivated by Ni and Co doping in β-MoB_2. *Int. J. Refract. Met. Hard Mater.* **2023**, *110*, 105997.
(46) Jaffray, J. Une nouvelle transition des cristaux de bichromate d'ammonium. *Journal de Physique et le Radium* **1952**, *13*, 430−430.
(47) Chakoumakos, B. C.; Paranthaman, M. Neutron powder diffraction study of the superconducting quaternary intermetallic compound YNi_2B_2C. *Physica. Section C: Superconductivity* **1994**, *227*, 143−150.
(48) Rundqvis, S.; Pramatus, S. Crystal structure refinements of Ni_3B, *o*-Ni_4B_3 and *m*-Ni_4B_3. *Acta Chem. Scand.* **1967**, *21*, 191.

https://doi.org/10.1021/acsomega.2c07523
ACS Omega 2023, 8, 9265−9274